

Assessment of cloud particle types in a deep convective environment using active remote sensing – a case study

S. ANDREI^{a*}, F. ȚOANCĂ^a, A. DANDOCȘI^{a,b}, L. BELEGANTE^a, A. NEMUC^a, L. MĂRMUREANU^a,
V. VULTURESCU^b, G. FLORESCU^c, D. NICOLAE^a

^aNational Institute of R&D for Optoelectronics, Bucharest-Măgurele, 077125, Romania

^bUniversity Politehnica of Bucharest, Bucharest, RO-060042, Romania

^cNational Institute for Research and Development in Informatics, Bucharest, 011455, Romania

This study documents a case of convective cloud system detected over Măgurele site, using lidar and ceilometer instruments. Cloud microphysical properties were examined by using the profiles of lidar ice to liquid water ratio derived from the RALI lidar together with the profiles of the temperature and the specific cloud ice and liquid water content derived from the ECMWF ERA Interim reanalysis. The obtained results emphasize the ability of polarization lidar to capture both micro-physical properties and macro-physical features of a convective cloud in its mature stage.

(Received November 25, 2016; accepted October 10, 2017)

Keywords: Lidar depolarization, Ceilometer, Convective mixed-phase clouds, Meteorology

1. Introduction

Clouds represent an important part of the climate system since their presence is affecting the amount of sunlight that reaches the earth surface. However, according to the Intergovernmental Panel on Climate Change [1], cloud feedbacks continue to be the largest source of uncertainty in global climate models estimates of Earth's climate sensitivity. Considering this, a proper understanding of clouds occurrence, evolution, typology, coverage and their macro- and micro-physical processes is very important.

The phase composition and micro-physical structure of clouds define the manner in which they modulate atmospheric radiation [2]. Mixed-phase cloud systems, containing both liquid particles in multiple phases and ice crystals, are frequently present in the Earth's atmosphere. Their life cycles are supported by the atmospheric motions that contribute to aerosol nucleation processes, causing cloud droplets and ice crystals formation. These cloud types represent a significant component of the atmosphere, with an average global coverage of 20 to 30% [3]. Previous studies have shown that the temperature at which these cloud types can be found ranges from -40°C [4], [5], to -9°C [6] according to model schemes. Observations reveal liquid water at temperatures as cold as -40°C [7], [8], [9], [10].

Remote sensing observations were used in different studies to distinguish between different cloud types and their features such as liquid to ice water content, ice crystals formation and precipitation. Various scientific activities like stationary and airborne campaigns: ACCEPT [11], BACCHUS [12], ASTAR [13], continuous observational data collected within the European Cloud observational Network CLOUDNET [14] or satellite based

measurements [15], [16] make use of active and passive remote sensing instruments to study cloud evolution and atmospheric processes that are responsible for cloud formation. In this context, lidars are active remote sensing instruments that are able to probe from few tens of centimeters to several meters above the cloud base, where the maximum cloud super-saturation occurs [17]. Considering this, any microphysical information potentially provided by lidar observations is of great value [18], [19]. Measurements of atmospheric depolarization using lidar were used to distinguish between liquid and solid phases of water in the atmosphere [20], [21], [22]. Ice crystals, considered non spherical particles can exhibit depolarization ratios greater than 0.2 [23], and can be easily used to distinguish between cloud droplets or super cooled droplets with low depolarization ratios and ice particles. In comparison, for continuous measurements, ceilometers are used to detect the cloud base for altitudes where the backscattered signal is strong [24], [25]. Although ceilometers can provide a limited set of optical parameters, they are able to cover extended time periods (including rain episodes).

This study is based on the use of remote sensing data provided by lidar and ceilometer analyzed together with meteorological data provided by ECMWF ERA Interim reanalysis. The cloud particle types were assessed in a deep convective environment. By using the volume linear depolarization ratio (VDR) provided by the lidar, a first estimation of the ice to liquid water ratio can be extracted. In combination with the ECMWF model, the meteorological context and the atmospheric behavior is studied with regard to the cloud particles (ice, super cooled water droplets and water droplets) found within a particular mixed-phase cloud. The paper is organized as follows: in section 2 the instruments and methodology

used to detect and study the microphysical properties of a convective cloud are described, the results are discussed in section 3, and conclusions are presented in section 4.

2. Instruments and methodology

The measurements were conducted using the multiwavelength depolarization Raman lidar (RALI) and the VÄISALA CL 31 Ceilometer, both located at Măgurele (44.35°N/26.03°E). Cloud phase features derived from these remote sensing instruments were analyzed within the meteorological context using ECMWF - ERA Interim reanalysis.

2.1. The multi-wavelength Raman lidar

The RALI instrument is located in a pre-urban site south-west of Bucharest. Since 2007 the instrument is part of the European Lidar Network - EARLINET performing systematic measurements according to a predefined schedule (two nighttime and one daytime measurement per week) [26]. The instrument complies with all quality assurance protocols required to operate in EARLINET [27]. Data used in this study is quality assured since all procedures in the EARLINET quality assurance program are applied both to the hardware and to the retrieved data.

The principle of lidar (light detection and ranging) is based on the detection of backscattered light that results from the interaction of the emitted laser light with the atmospheric particles. The laser light gives information on the optical and geometrical properties of the atmospheric constituents [28], [29], [30]. The multi-wavelength depolarization Raman lidar (RALI) used for this study is capable to detect the Raman backscatter radiation from nitrogen, and Mie / Rayleigh backscatter radiation from atmospheric molecules and aerosol particles, providing data products related to optical, microphysical and geometrical properties. The output parameters are the backscatter and extinction coefficient profiles (collected for 355-532-1064 nm for the first parameter, and 355-532 for the second parameter) and particle depolarization ratio profiles (at 532nm). The high dynamic range of the instrument is able to cover altitudes from 0.8 to 15 km, with a 3.75 m spatial resolution and 1 minute temporal resolution.

An important parameter derived from the lidar signals is the depolarization ratio (volume and particle linear depolarization ratios hereafter referred to as VDR and PDR) [31], [32]. These quantities enable the investigator to distinguish between spherical particles (characterized by low depolarization ratios), and non-spherical particles (with higher depolarization ratios). RALI is able to measure the parallel and cross components at 532nm. This wavelength ensures the capability to detect not only coarse aerosol particles but also ice, water and mixed-phase cloud particles [28]. The depolarization products are usually used to distinguish between several aerosol types. In case of aerosol typing studies, the PDR is commonly used since this parameter only accounts for the aerosol type and not the amount of aerosol in the investigated layer (intensive

parameter). For pure mineral dust particles, the PDR value at 532 nm ranges from 0.3 to 0.39 while for dust mixtures PDR values are from 0.1 to 0.3. For biomass burning particles, the 532nm PDR ranges around 0.08 and 0.15 and for marine aerosols the PDR values increase up to 0.06 [33], [34], [35]. The study of mixed-phase cloud dynamics requires the use of high resolution lidar products. A suitable option is to use the VDR since the high temporal and vertical resolution of this parameter can provide information on cloud dynamics and structure. The use of PDR retrievals imply additional lidar products (backscatter coefficient) that require longer integration times and therefore lower temporal resolution, making this study more difficult. For liquid to ice water content studies, the VDR can provide a better vertical and temporal resolution since the additional lidar products are not required. VDR values are affected by the amount of particles to be investigated (extensive parameters) but these studies do not require absolute values. In the case of water droplets occurrence, the VDR is low, since water droplets do not change the polarization degree, while for ice crystals, the VDR can increase well above 0.4 [36].

2.2. The CL31 Ceilometer

The VÄISALA CL31 Ceilometer is able to perform continuous measurements at 910 nm in all weather conditions. It is capable to detect up to three cloud levels and can also provide the attenuated backscatter profiles. The instrument can provide raw data profiles with a time resolution of 16s, a vertical resolution of 5m and a maximum altitude better than 7.5km [37]. A detailed description of the instrument is given in [38]. The instrument is situated in the vicinity of the lidar measurement site - several hundred meters away.

2.3. The ECMWF ERA-Interim reanalysis

A complex meteorological analysis was performed on different spatial scales (synoptic, mesoscale and local), for better understanding and interpretation of the physical processes that contribute to the occurrence and evolution of mixed-phase clouds.

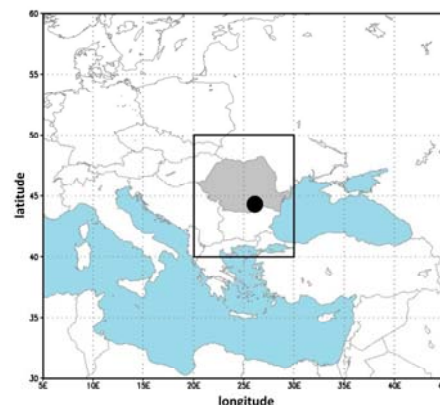


Fig. 1. Meteorological scales used in this study: synoptic (entire window), mesoscale (black quadrant), and local (black dot)

The ECMWF ERA-Interim reanalysis database [39] at a horizontal resolution of $0.125^\circ \times 0.125^\circ$ was used. Synoptic analysis of geopotential height and temperature at significant atmosphere's levels on a latitude-longitude atmospheric window of $30^\circ - 60^\circ \text{ N}$ and $5^\circ - 45^\circ \text{ E}$ (Fig.1), was used in order to assess atmospheric circulations and thermal advections.

The interpretation of the presence of different cloud types detected by the lidar, was based on the mesoscale analysis of low, medium and high cloud cover performed on a $40^\circ - 50^\circ \text{ N} / 20^\circ - 30^\circ \text{ E}$ window (Fig.1, black quadrant). The local analysis was focused on a small grid box (Fig.1, black dot), which included the location of the remote sensing instruments. Profiles of temperature (T), specific cloud ice water content (CIWC) and specific cloud liquid

water content (CLWC) were analyzed and compared with the lidar derived products. Meteorological data have been selected in a way to remain close-in-time to the remote sensing measurements.

3. Results and discussion

On May 16th 2014, lidar measurements above Măgurele had emphasized the presence of a convective cloud with a gradual vertical expansion (Fig.2). The Range Corrected Signal (RCS) time series (Fig. 2 left) show the vertical extent and temporal evolution of the cloud system.

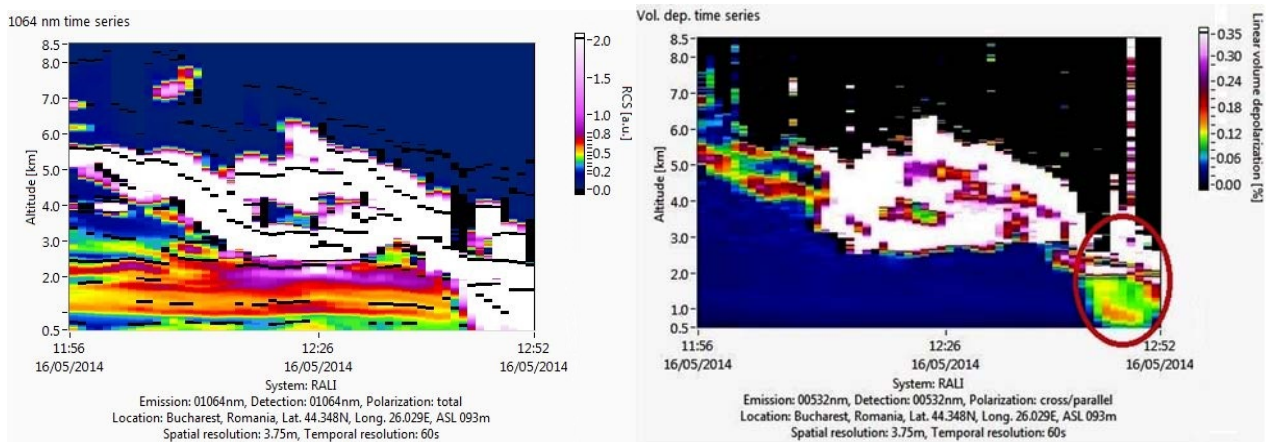


Fig. 2. Lidar times series of range corrected signal at 1064 nm (left) and volume linear depolarization (right), on May 16, 2014

The optical thickness (OT) at 532nm show values higher than 4 within the cloud layer, indicating that the cloud consists probably of high water content. For high density clouds (usually with OT higher than 3) multiple scattering effects are likely to affect the lidar products. Since for this study only qualitative information is required to assess the ice-to-liquid water content, it is shown that these effects could be disregarded.

The VDR time series (Fig. 2 right) show high vertical and temporal dynamics of the cloud layers with values ranging from 0.1 to 0.35. These values indicate the presence of a mixed-phase cloud regime, typical for storm related events [7]. High VDR value indicates the presence of non-spherical particles that most probably are ice particles. The time series in Fig 2 emphasize that in less than one hour the cloud base decreased from 5 to 2km altitude. During the last ten minutes of measurements (between 12:42 and 12:52 UTC) the lidar instrument detected the initiation of the heavy rain event, (red circle in Fig. 2 left).

The ceilometer time series (Fig.3) depicts the entire episode of the storm passing over the measurement site. Red circle (Fig.3) corresponds to the initiation of precipitation event, indicated in Fig. 2, right. It can be noticed that even if the lidar measurements are limited by the rain event, the ceilometers is still able to provide information on the extent of the rain event. High

attenuated backscatter values detected during the entire event (above $9 \cdot 10^{-5} \text{ sr}^{-1} \times \text{m}^{-1}$) can give an insight on the extent of the storm, in terms of precipitation rate.

The detected cloud base shows similarities with the one determined from the lidar time series of range corrected signals (Fig.2, left). The lack of signal between 2 and 4.5km around 13:00 UTC, indicates high density cloud particles. The initiation of precipitation event (Fig. 3, red circle) is in accordance with the lidar measurements.

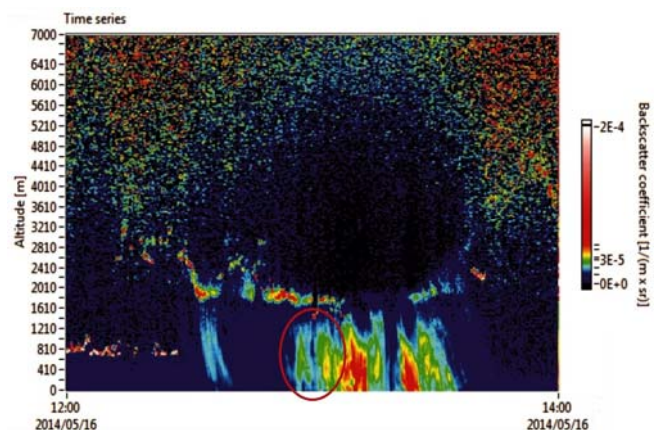


Fig. 3. Image of convective cloud evolution and storm event provided by VÄISALA CL 31 Ceilometer on May 16, 2014

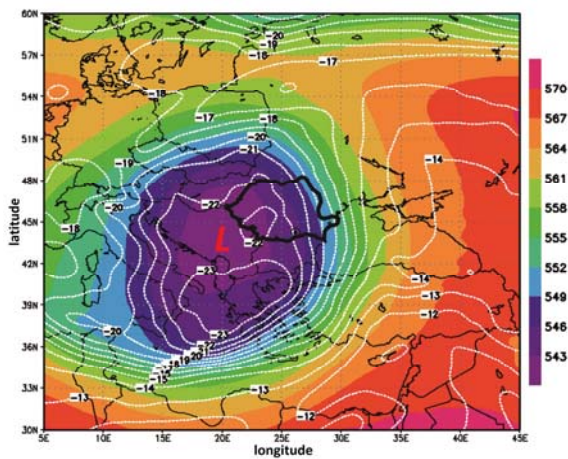


Fig. 4. ECMWF ERA - Interim reanalysis of geopotential height at 500 hPa (color palette) and temperature °C (white contours) for May 16, 2014 [12TC]

In order to provide an overall impression on the atmospheric behaviour during the studied case, a multiscale analysis of the meteorological context was performed. The synoptic scale analysis (Fig.4) for 16th of May 2014, reveals the presence of a strong cyclonic area, developed over Mediterranean Sea, with direct influence on territory of Romania. The cut-off low enabled the advection of a cold humid air-mass towards the measurement site.

The meteorological conditions favored the development of multi-layered cloud systems, as it was indicated by the model mesoscale reanalysis of cloud fraction coverage (Fig.5). The medium and high cloud cover over Bucharest area (Fig. 5, black quadrant) is consistent with the lidar measurements (Fig.2).

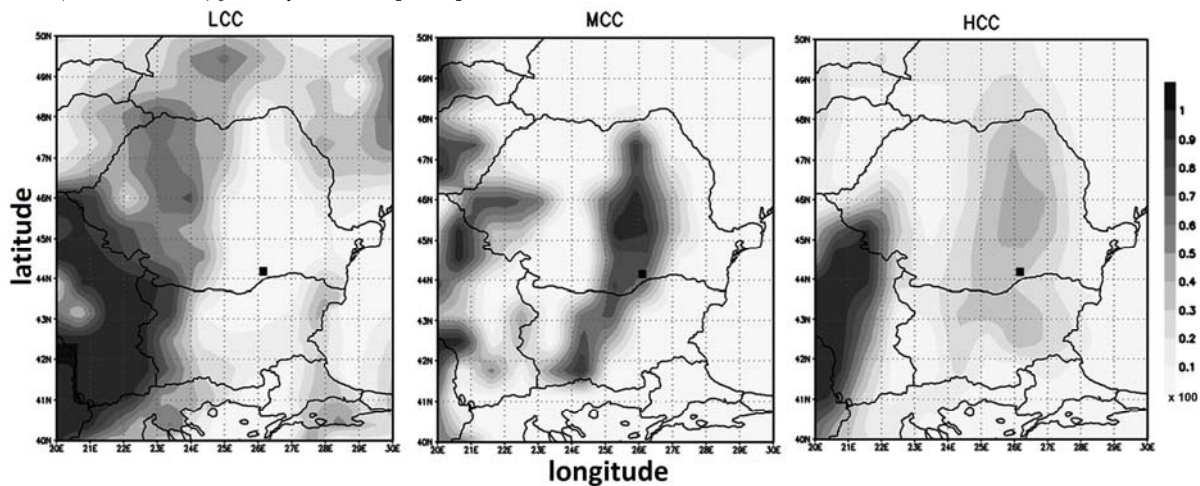


Fig. 5. Low Cloud Cover (LCC) - left, Medium Cloud Cover (MCC) - center, and High Cloud Cover (HCC) - right (greyscale %) over the region of interest, derived from ECMWF ERA - Interim reanalysis for May 16, 2014 [12TC]

The temperature profile (Fig. 6, black line) derived from the model data, depicts the state of atmospheric environment close to the measurement location: thermal profile shows a strong decrease with altitude. The freezing level is located at 775 hPa, which approximately corresponds to 2 km. Within the layer between 775 and 500 hPa (2 – 5 km), the thermal gradient has a value of -22 °C, whilst above the 500 hPa the temperature continues the decreasing until -48 °C is reached at the 300 hPa level (≈9km altitude).

The vertical distribution of humidity is detailed through the profiles of specific ice and liquid cloud water content (Fig.6, red and blue lines). The maximum CLWC of 45 μg/kg is indicated at 900 hPa (≈ 1km), then the parameter marks a strong decrease between 875 and 500 hPa. The profile of CIWC shows a remarkable increase between 775 and 275 hPa with a maximum value of 27 μg/kg at 350 hPa (≈ 8km). This peak is related to the Cumulonimbus cloud top, where the dominant particles types are ice crystals.

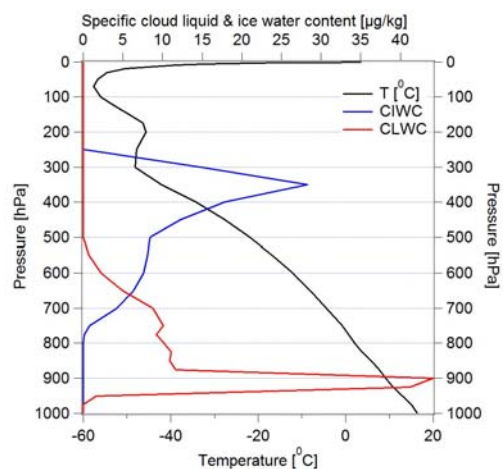


Fig. 6. Profiles of temperature (black line), specific cloud ice (blue line) and liquid (red line) water content at Măgurele derived from ECMWF ERA – Interim reanalysis for May 16, 2014 [12TC]

Lidar measurements (Fig. 2) are in a good agreement with the specific cloud ice and liquid water content derived from ECMWF ERA Interim reanalysis for Măgurele (Fig. 6). The temperature profile (Fig. 6, black line) show values of 0°C to -25°C for the layer between 2 and 6 km altitudes (corresponding to the atmospheric layer between 775 and 450 hPa), which are also in a good agreement with previous studies [7], [8]. Below 2 km, both the lidar and ECMWF profiling data, indicate the presence of water droplets since the VDR show values lower than the values measured in the cloud (Fig. 2 right, red circle), coupled with positive temperature and high values of CLWC. The region of cloud detected by the lidar between 4 and 5 km (11:56 – 12:11 UTC) presents a ratio of 0.1 to 0.2 (Fig. 2 right), corresponding with super-cooled water droplets, since the temperature values are negative and the CIWC values are increasing (Fig. 6). During the next time interval (12:11 – 12:41 UTC) the cloud layer between 2.5 and 6 km presents VDR values above 0.3 (Fig. 2 right) indicating the dominant presence of ice crystals while the temperature and CIWC profiles in Fig 6 confirm this assumption.

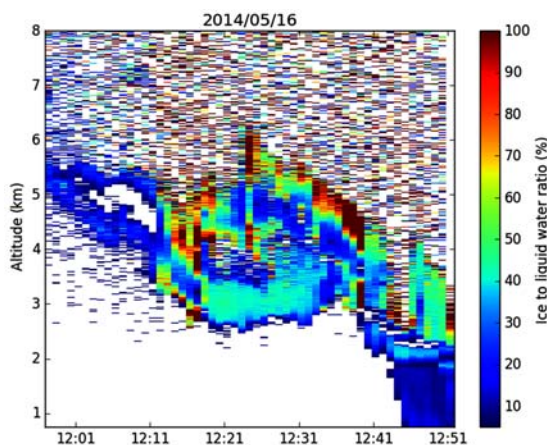


Fig. 7. Time series of ice-to-liquid water ratio (0%=water, 100%=ice, in between is mixed-phase) derived from lidar measurements performed on May 16, 2014

Valuable information is provided by the time series of ice-to-liquid water ratio derived from lidar data (Fig. 7), which captures the storm motion, as it approaches the measurement site, revealing both micro- and macro-physical features of the convective storm. During the first time interval (11:56 – 12:11 UTC), lower values of ice-to-liquid water ratio (10 to 30%) emphasize a region with water and super-cooled water droplets at 4 to 6 km altitude, characteristic to the wall cloud part of a convective cell. Higher values of ice-to-liquid water ratio (30 to 100%) at the altitudes between 2.7 and 6 km, during 12:11 - 12:41 UTC, indicate a mixture of particles (water droplets, super-cooled water and ice particles). For the last time interval (12:41 – 12:51 UTC), lower values of 10 to 20% are visible at the altitudes of 1 to 2 km corresponding to the precipitation area, while above 2 km the ice to liquid water ratio shows higher values (above 50%). An

important macro-physical feature of convective clouds is revealed, namely the presence of updrafts (visible during 12:11 and 12:16 time interval) and downdrafts (visible after 12:35 UTC).

The vertical distribution of cloud particle types in Fig. 7 is consistent with the vertical profiles of the temperature and the specific cloud liquid and ice content in Fig. 6. The higher values of CLWC indicated between the surface and 800 hPa (where the air temperature is positive) correspond to the precipitation area. The layer between 800 and 500 hPa (where the values of CLWC are decreasing, while the values of CIWC are increasing, and the temperature decreases from 0°C to -22°C) corresponds to the mixed-phase cloud area. Up to the level of 500 hPa, the CIWC is increasing, suggesting the predominance of ice the particles. The vertical distribution of cloud particles for this case is consistent with those mentioned by literature [40, 41, 42].

4. Conclusions

The results presented and discussed in this study, demonstrate the capability of the lidar instruments to detect the multiple cloud layers. From our knowledge this is the first study performed on a convective cloud by using lidar measurements, emphasizing also its dynamics throughout the up-and-downdraft motions. Through its instability, the synoptic meteorological conditions had supported the development and evolution of convective clouds.

The lidar-derived VDR profiles allow to distinguish between the spherical (water droplets) and the non-spherical (ice particles) constituents of clouds. As the lidar measurements are limited by the rain event, the simultaneous use of ceilometer complemented the image of the event providing information on the extent of the rain.

The ice-to-liquid water ratio profiles obtained from the lidar measurements are in a good agreement with the specific cloud ice and liquid water content obtained from the ECMWF reanalysis data. The temperature range for the mixed-phase in the studied case is in accordance with previous studies.

Acknowledgements

The research leading to these results has received funding from Romanian Partnerships Program in priority areas PN II, implemented by MEN UEFISCDI, project no. 144/2014 - LIRA, ANCS Core Program, project no. 16.40.01.01, the Romanian National Authority for Scientific Research, Program for Research - Space Technology and Advanced Research – STAR Program project no. 55/2013 – CARESSSE and the European Union's Horizon 2020 Research and Innovation Programme, under Grant Agreement no 692014 - ECARS.

The authors would like to thank Professor Dr. Sabina Ștefan (University of Bucharest, Faculty of Physics) for providing the ceilometer dataset.

References

- [1] Intergovernmental Panel on Climate Change (2013), Chapter 7 of the fifth assessment report of the Intergovernmental Panel on Climate Change. [http://www.climatechange2013.org/images/uploads/WGIAR5_WGI2Doc2b_FinalDraft_Chapter07.pdf].
- [2] M. D. Shupe, J. S. Daniel, G. de Boer, E. W. Eloranta, P. Kollias, E. Luke, C. N. Long, D. D. Turner, J. Verlinde, *Bull. Amer. Meteor. Soc.* **89**, 1549 (2008).
- [3] S. G. Warren, C. J. Hahn, J. London, R. M. Chervin, R. L. Jenne (1988), Global Distribution of Total Cloud Cover and Cloud Type Amounts Over the Ocean, NCAR Tech. Note NCAR/TN-317 + STR, Natl. Cent. for Atmos. Res., Boulder, Colo. (1988).
- [4] A. D. Del Genio, M-S. Yao, W. Kovari, K. K-W. Lo, *J. Climate* **9**, 70 (1996).
- [5] T. Ose, *J. Meteor. Soc. Japan* **71**, 93 (1993).
- [6] D. Gregory, D. Morris, *Climate Dyn.* **12**, 641 (1996).
- [7] R. M. Rauber, L. O. Grant, *J. Climate Appl. Meteor.* **25**, 489 (1986).
- [8] A. J. Heymsfield, L. M. Miloshevich, A. Slingo, K. Sassen, D. O'C. Starr, *J. Atmos. Sci.* **48**, 923 (1991).
- [9] J. M. Intrieri, M. D. Shupe, T. Uttal, B. J. McCarty, *J. Geophys. Res.* **107**, 8030 (2002).
- [10] A. Korolev, G. Isaac, S. G. Cober, J. W. Strapp, J. Hallett, *Quart. J. Roy. Meteor. Soc.* **129**, 39 (2003).
- [11] A. Myagkov, P. Seifert, U. Wandinger, R. Bühl, Engelmann, *Atmos. Meas. Tech.* **9**, 3739 (2016).
- [12] <http://www.bacchus-env.eu/>
- [13] J.-F. Gayet, I. S. Stachlewska, O. Jourdan, V. Shcherbakov, A. Schwarzenboeck, R. Neuber, *Ann. Geophys.* **25**, 1487 (2007).
- [14] A. J. Illingworth, R. J. Hogan, E. J. O'Connor, D. Bouniol, J. Delanoë, J. Pelon, A. Protat, M. E. Brooks, N. Gaussiat, D. R. Wilson, D. P. Donovan, H. K. Baltink, G.-J. van Zadelhoff, J. D. Eastment, J. W. F. Goddard, C. L. Wrench, M. Haeffelin, O. A. Krasnov, H. W. J. Russchenberg, J.-M. Piriou, F. Vinit, A. Seifert, A. M. Tompkins, U. Willén, *Cloudnet*, *B. Am. Meteorol. Soc.* **88**, 883 (2007).
- [15] D. Zhang, Z. Wang, D. Liu, *J. Geophys. Res.-Atmos.* **115**, D00H13 (2010).
- [16] J. Bühl, A. Ansmann, P. Seifert, H. Baars, R. Engelmann, *Geophys. Res. Lett.* **40**, 4404 (2013).
- [17] M. Pinsky, A. Khain, I. Mazin, A. Korolev, *J. Geophys. Res.* **117**, D18211 (2012).
- [18] U. Lohmann, J. Feichter, *Atmos. Chem. Phys.* **5**, 715 (2005).
- [19] A. McComiskey, G. Feingold, A. Shelby Frisch, D. D. Turner, M. A. Miller, J. C. Chiu, Q. Min, J. A. Ogren, *J. Geophys. Res.* **114**, D09203 (2009).
- [20] R. M. Scotland, K. Sassen, R. Stone, *J. Appl. Meteor.* **10**, 1011 (1971).
- [21] K. Sassen, *Bull. Am. Meteor. Soc.* **72**, 1848 (1991).
- [22] S. R. Pal, A. I. Carswell, OSA Publishing, *Applied Optics* **12**, 1530 (1973).
- [23] J. M. Intrieri, M. D. Shupe, T. Uttal, B. J. McCarty, *J. Geophys. Res.* **107**, 8030, (2002).
- [24] K. Van Tricht, I. V. Gorodetskaya, S. Lhermitte, D. D. Turner, J. H. Schween, N. P. M. Van Lipzig, *Atmos. Meas. Tech.* **7**, 1153 (2014).
- [25] P. V. Hobbs, A. L. Rangno, Q. J. Roy, *Meteorol. Soc.* **124**, 2035 (1998).
- [26] G. Pappalardo, A. Amodeo, A. Apituley, A. Comeron, V. Freudenthaler, H. Linné, A. Ansmann, J. Bösenberg, G. D'Amico, I. Mattis, L. Mona, U. Wandinger, V. Amiridis, L. Alados-Arboledas, D. Nicolae, M. Wiegner, *Atmos. Meas. Tech.* **7**, 2389 (2014).
- [27] M. Sicard, G. D'Amico, A. Comeron, L. Mona, L. Alados-Arboledas, A. Amodeo, H. Baars, J. M. Baldasano, L. Belegante, I. Biniotoglou, J. A. Bravo-Aranda, A. J. Fernández, P. Fréville, D. García-Vizcaíno, A. Giunta, M. J. Granados-Muñoz, J. L. Guerrero-Rascado, D. Hadjimitsis, A. Haefele, M. Hervo, M. Iarlori, P. Kokkalis, D. Lange, R. E. Mamouri, I. Mattis, F. Molero, N. Montoux, A. Muñoz, C. Muñoz Porcar, F. Navas-Guzmán, D. Nicolae, A. Nisantzi, N. Papagiannopoulos, A. Papayannis, S. Pereira, J. Preißler, M. Pujadas, V. Rizi, F. Rocadenbosch, K. Sellegri, V. Simeonov, G. Tsaknakis, F. Wagner, G. Pappalardo, *Atmos. Meas. Tech.* **8**(11), 4587 (2015).
- [28] V. A. Kovalev, W. E. Eichinger, *Elastic Lidar: Theory, Practice, and Analysis Methods*, Wiley Interscience, ISBN 0-471-20171-5. (2004).
- [29] A. Timofte, L. Belegante, M. M. Cazacu, B. Albina, C. Talianu, S. Gurlui, *J. Optoelectron. Adv. M.* **17**(7-8), 911 (2015).
- [30] L. Belegante, D. Nicolae, A. Nemuc, C. Talianu, C. Derognat, *Acta Geophysica*, **62**(2), 276 (2014).
- [31] V. Freudenthaler, *Atmos. Meas. Tech.* **9**, 4181 (2016).
- [32] J. A. Bravo-Aranda, L. Belegante, V. Freudenthaler, L. Alados-Arboledas, D. Nicolae, M. J. Granados-Muñoz, J. L. Guerrero-Rascado, A. Amodeo, G. D'Amico, R. Engelmann, G. Pappalardo, P. Kokkalis, R. Mamouri, A. Papayannis, F. Navas-Guzmán, F. J. Olmo, U. Wandinger, F. Amato, M. Haeffelin, *Atmos. Meas. Tech.* **9**, 4935 (2016).
- [33] A. Petzold., M.E. ICAROHS - Inter-Comparison of Aerosol Retrievals and Observational Requirements for Multi-wavelength HSRL Systems. (2010).
- [34] S. Gross, M. Esselborn, B. Weinzierl, M. Wirth, A. Fix, A. Petzold, *Atmos. Chem. Phys.* **13**(5), 2487 (2013).

- [35] S. P. Burton, R. A. Ferrare, C. A. Hostetler, J. W. Hair, R. R. Rogers, M. D. Obland, C. F. Butler, A. L. Cook, D. B. Harper, K. D. Froyd, *Atmos. Meas. Tech.* **5**, 73 (2012).
- [36] K. Sassen, Polarization in lidar, in: *Lidar*, edited by: Weitkamp C., vol. 102 of Springer Series in Optical Sciences, 19–42, Springer, New York (2005).
- [37] P. Sokół, I. Stachlewska, I. Ungureanu, S. Ștefan, *Acta Geophysica*, **62**(2), 367 (2014).
- [38] C. Munkel, *Meteorologische Zeitschrift* **16**(4), 451 (2007)
- [39] D. P. Dee, S. M. Uppala, A. J. Simmons, P. Berrisford, P. Poli, S. Kobayashi, U. Andrae, M. A. Balmaseda, G. Balsamo, P. Bauer, P. Bechtold, A. C. M. Beljaars, L. van de Berg, J. Bidlot, N. Bormann, C. Delsol, R. Dragani, M. Fuentes, A. J. Geer, L. Haimberger, S. B. Healy, H. Hersbach, E. V. Hólm, L. Isaksen, P. Kallberg, M. Köhler, M. Matricardi, A. P. McNally, B. M. Monge-Sanz, J.-J. Morcrette, B.-K. Park, C. Peubey, P. de Rosnay, C. Tavolato, J.-N. Thépaut, F. Vitart, Q. J. R. *Meteorol. Soc.* **137**, 553 (2011).
- [40] H. R. Pruppacher, J. D. Klett, *Microphysics of Clouds and Precipitation*, D. Reidel Publishing Company, Boston, 714 pp., 1978.
- [41] R. R. Rodgers, *A Short Course in Cloud Physics*, 2nd Edition. Pergamon Press, New York, 116 pp., 1979.
- [42] C. D., Ahrens, *Meteorology Today, An Introduction to Weather, Climate, and the Environment*. Brooks/Cole Thomson Learning, 182 pp. (2000).

*Corresponding author: simona.andrei@inoe.ro